NUMERICAL SIMULATIONS OF IMPACTS OF A SPHERICAL SHELL PROJECTILE ON SMALL ASTEROIDS. K. Kurosawa[1], H. Senshu[1], K. Wada[1], and TDSS team, Planetary Exploration Research Center, Chiba Institute of Technology, (kosuke.kurosawa@perc.it-chiba.ac.jp)

Introduction: Recently, impactors have been widely used in a number of planetary exploration missions [e.g., 1-4] to excavate the fresh material from underground of asteroids, which are expected not to suffer space weathering and thermal alteration due to solar incidence.

The prediction of impact outcomes is necessary to derive scientific results as much as possible. There are two problems, however, to predict impact outcomes on small asteroids. First, the mechanical properties of asteroids, such as the bulk porosity and the yield strength, are largely unknown prior to arriving near target asteroids. Asteroids have a variation of the porosity from 0% to 80 % [5]. Rocky materials have a wide range of the yield strength Y depending on its condition. For example, typical values of Y for granular materials and a rigid rock are 0.01 MPa and 10 MPa, respectively. Second, the shape of impactors is highly limited in planetary exploration missions. The impact processes have been understood based on the results of impact experiments and numerical calculations with dense, spherical projectiles. In contrast, hollow projectiles have been often used in the previous missions [1, 2, 4]. HAYABUSA-2, the Japanese ongoing asteroid exploration mission, has a plan to shoot a half-spherical shell projectile, which is called a small carry-on impactor (SCI) [e.g., 7]. According to the recent impact experiments using a hollow projectile, the angle distribution of ejecta is largely different from the case of dense ones [8]. This means that we do not know the nature of a flow field driven by an irregular shaped projectile.

In this study, we numerically simulated the excavation processes by a half-spherical shell projectile on highly-porous small asteroids to investigate the impact outcomes by such irregular shaped projectiles on porous media.

Numerical model: We used the iSALE shock physics code [9-11] in this study. Here, we summarized the calculation conditions that almost fit the impact of SCI. A copper half-spherical shell and a uniform granite layer were set as a projectile and a target in a cylindrical coordinate. The impact velocity was fixed at 2 km/s. The Tillotson EOS for copper [12] and the ANEOS for granite [13] were employed. The Johnson-Cook strength model with the parameters for copper [14] was used for the projectile. One of the most simple strength models (Drucker-Prager model [15]) was used for the target in this study. The yield strength of the target Y is given by $Y = \max(Y_{coh} + \mu P, Y_{limit})$, where Y_{coh}, μ, P, and Y_{limit} are the cohesion in the target, the coefficient of internal friction, the pressure in the target, and the Hugoniot elastic limit of the target. We employed the ε–α compaction model [11] to investigate the effects of the target porosity on the excavation processes. No gravity was included into the calculation. Lagrangian tracer particles were inserted into the grids to investigate the impact-driven flow field. For reference, we also conducted a few simulations using a dense copper spherical impactor with the same mass under the same conditions.

Results: Examples of snapshots of the simulation are shown in Fig. 1. A projectile penetration, shockwave propagation, and a cavity growth are clearly observed. The penetration depth of the dense sphere at a given time is larger than that of the half spherical shell even though the mass of both projectiles are the same. We investigated the change in the kinetic energy of the impactor as shown in Fig. 2a. Although a penetrating projectile is highly deformed due to ram pressure from the target, it penetrates into the target as a single object, like a plate, as shown in Fig. 1. Thus, an averaged value of the vertical component of the particle velocity of the tracer particle nearest to the symmetric axis was employed as a projectile velocity

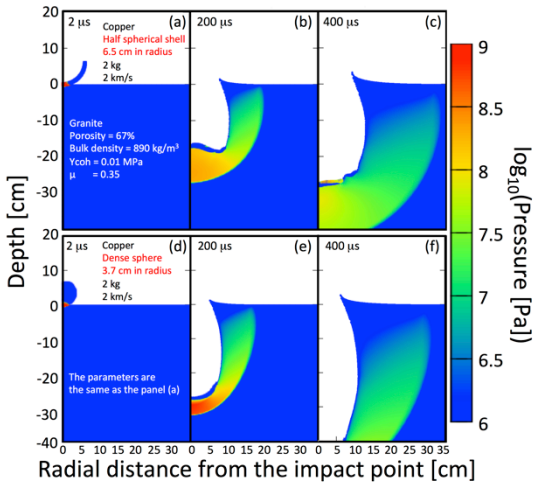

Figure 1. Snapshots of the simulation. Panels (a)-(c) and (d)–(f) show the results for a half spherical shell projectile and a dense sphere, respectively. The pressure contour is shown. The time after the initial contact are indicated in the figure. The material parameters used in this calculation are shown in panels (a) and (d).

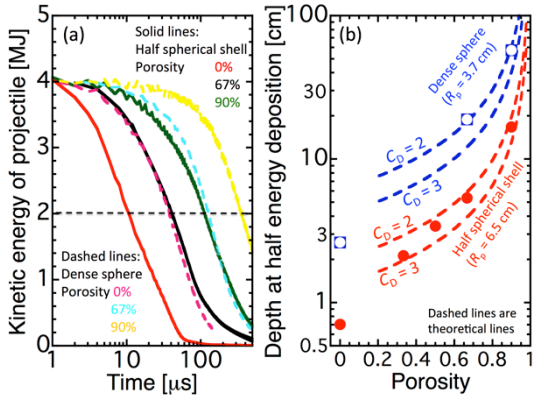

Figure 2. (a) The change in the kinetic energy of the projectile for each shape of the projectile and the target porosity. (b) The projectile depth at a half energy deposition as a function of the target porosity.

because such tracers has nearly zero velocity to the radial direction. The energy transfer from the projectile to the target by a half spherical shell occurs at an earlier stage of the penetration at a given target porosity. Figure 2b shows the depth of the projectile where a half of the initial kinetic energy remains. We can derive an effective drag coefficient C_D by a comparison between the simulation results and analytical solutions for the deceleration rate of a penetrating object under the inertial resistance from the target [e.g., 16]. The change in the projectile velocity is given by $\Delta v/\Delta t = -(1/2)\rho_t C_D \pi r_p^2 v^2/m_p$, where v, t, and ρ_t , r_p and m_p are the projectile velocity, the time after the initial contact, the initial bulk density of the target, the initial radius of the projectile, and the initial mass of the projectile, respectively. We found that the results are reproduced well at C_D = 2-3 in the case of both a half spherical shell and a sphere. Note that C_D defined in this study includes the effect of the change in the cross section of the projectile due to deformation and the increase in the target density by a compaction due to a precursive shockwave on a projectile deceleration.

Figure 3 shows the velocity and angle distribution of the target materials at a depth within 1 cm from the surface as a function of the radial distance from the impact point. We extracted the maximum of the particle velocity u_{pmax} in the simulation using tracer particles. According to simulations with Y_{coh} varied from 0.01 MPa to 10 MPa, not shown in this abstract, the u_{pmax} can be approximated as the ejection velocity of the target materials near the surface v_{eject} if Y_{coh} is lower than 0.1 MPa. The v_{eject} for a half spherical shell at a given distance and a target porosity is higher than that for a dense sphere. The v_{eject} distribution at >20 cm can be approximated straight lines on a log-log plot. Although the power law exponent n decreases as the target porosity increases, n does not strongly depends on the shape of the projectile.

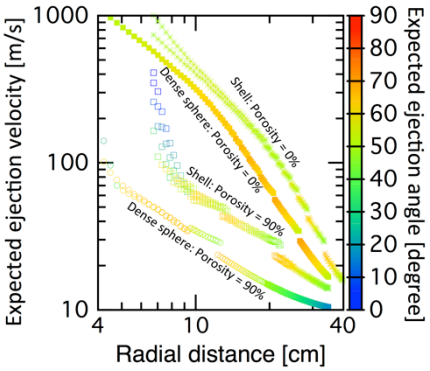

Figure 3. The velocity and angle distribution of the target materials near the surface.

Discussion and Conclusions: The shape of projectiles clearly affects the energy transfer rate from the projectile to the target as shown in Fig. 2a. The energy deposition at an early stage of the penetration may lead to a higher ejection velocity as shown in Fig. 3. Since C_D for a half spherical shell is similar to that for a dense sphere, the difference in the rate is expected to be caused solely by a larger cross section of a half spherical shell than a dense sphere. Although the controlling physics to determine the accurate value of C_D should be explored in the future work, an empirical value derived in this study may be useful to design an operating plan for exploration missions.

Acknowlegements: We appreciate the developers of iSALE, including G. Collins, K. Wünnemann, B. Ivanov, J. Melosh, and D. Elbeshausen.

References: [1] Foing, B. H., et al. (2001), *Earth Moon Planets*, **85-86**, 523. [2] A'Hearn, M. F., et al. (2005), *Science*, **310**, 258. [3] Yano, H. et al. (2006), *Science*, **312**, 1350. [4] Heldmann et al. (2011), *SSR*, **167**, 93. [5] Consolmagno, G. J. et al. (2008), *Chem. Erde (Geochem.)* 68, 1. [6] Kadono, T. (1999), *PSS*, **47**, 305. [7] Wada, K. et al. (2014), *LPS XXXXV*, 1768. [8] Schultz, P. H. et al. (2010), *Science*, **330**, 468. [9] Amsden A. A., et al. (1980) *LANL Report* LA-8095. 101 p. [10] Ivanov B. A., et al. (1997), *IJIE*, **20**, 411. [11] Wünnemann, K., et al. (2006), *Icarus*, **180**, 514. [12] Tillotson, J. H. (1962), *Technical Report GA-3216*, General Atomic Report. [13] Thompson, S. L., and Lauson, H. S. (1972), Rep. SC-RR-71-0714, Sandia Natl. Lab., Albuquerque, N. M. [14] Johnson G. R. and Cook W. H. (1983), *Proc. 7th International Symposium on Ballistics*. Hague, The Netherlands. [15] Drucker, D. C. and Prager, W. (1952), *Quarterly of Appl. Math.*, **10**, 157. [16] Okamoto, T. et al. (2013), *Icarus*, **224**, 209.